Article

Journal of the Brazilian Chemical Society

https://dx.doi.org/10.21577/0103-5053.20240078

J. Braz. Chem. Soc. **2025**, *36*, 1, e-20240078, 1-9

Pretreatment of *Oryza sativa* (Rice) and *Musa cavendishii* (Banana) Waste Biomass Using Ionic Liquids of Choline Amino Acid for Nanoscale Cellulose Production

Fabiane F. da Silva, [*,a] ***Danylo B. Mendes,*** [a] ***Patrícia M. Guarda,*** [a] ***Anselmo F. R. Rodriguez*** [b] ***and Emerson A. Guarda*** [a]

[a]*Laboratório de Química Ambiental, Universidade Federal do Tocantins, 77001-090 Palmas-TO, Brazil*

[b]*Departamento de Física, Universidade Federal do Acre, 69920-900 Rio Branco-AC, Brazil*

The species *Oryza sativa* (rice) and *Musa cavendishii* (banana) are sources of cellulose-rich waste biomass in the Amazon region, Tocantins State. This research investigates the nanoscale production of cellulose through the interactions between three choline amino acid ionic liquids Ch[AA]IL and the respective fibers by pretreatment. To this end, the synthesis of three ILs was carried out: choline arginate Ch[Arg], choline glycinate Ch[Gly] and choline lysinate Ch[Lys], characterized by Fourier transform infrared spectroscopy (FTIR). The samples resulting from the pretreatment were analyzed by scanning electron microscopy (SEM), transmission electron microscopy (TEM), X-ray diffraction (XRD) and thermogravimetric analysis (TGA). It was possible to infer from the SEM micrographs that Ch[Arg] caused greater fiber breakage than the other ILs. The TEM analyses identified fibers up to 16 nm in diameter. Positive effects were observed in the diffractograms, although no crystallinity was obtained in the pretreated samples. Thermogravimetry curves showed that the fibers treated with Ch[Arg] showed higher thermal stability.

Keywords: nanocellulose, ionic liquids, biomass, pretreatment

Introduction

Ionic liquids (ILs) can be defined simply as a liquid composed of ions.[1] They have been used in pretreatment, emerging worldwide as a new way to impart suitable physicochemical properties to biomass for use in the production of advanced bio-based products.[2] The use of ILs in nanocellulose (NC) production has gained significant interest due to the intrinsic physical solubility of cellulosic materials in many ILs, as these solvents are able to dissolve the amorphous portion of lignocellulosic biomass without destroying the crystalline regions.[3]

NC is a light and strong substance obtained from plant matter, which includes cellulose fibrils and crystals of nanometric size, and is classified into different nanomaterials such as (*i*) cellulose nanocrystals (CNCs), (*ii*) cellulose nanofibrils (CNFs) and (*iii*) bacterial cellulose (BC),[4] possessing high surface area, with exceptional properties such as biodegradable, low density and good mechanical properties.[5] Unlike CNCs, CNFs exhibit a long and flexible nanoscale structure containing crystalline and amorphous regions, usually showing a nanoscale width and a microscale length.[6]

Thus, a variety of approaches can be used to obtain NC, such as ultrasonic technique, enzymatic hydrolysis, besides acid hydrolysis,[5] however, these alkaline and acid methods have disadvantages such as corrosion of equipment, damage to the environment, besides the use of high-cost products.[7] Given these challenges, some pretreatments are being developed for biomass delignification using mild, green and sustainable solvents.[8] Choline amino acid ionic liquids Ch[AA]IL, represent a new class of ILs obtained from natural and renewable raw materials. These liquids are basically composed of the quaternary ammonium cation choline and an amino acid anion, such as glycinate and lysinate, for example.[9] They have been called also bio-ILs and reported in the scientific literature efficiently in the pretreatment of biomass;[10-12] however, to the best of our knowledge, no research has been conducted with these "green" solvents for nanoscale cellulose production using residual lignocellulosic biomass.

Lignocellulosic biomass comprises cellulose biopolymers and hemicellulose carbohydrates together with lignin,[13] cellulose being composed of repeated d-anhydroglucopyranose units linked by β-1,4-glycosidic

*e-mail: fabi_fernandes@uft.edu.br
Editor handled this article: Fernando C. Giacomelli (Associate)

bonds, with fascinating properties such as biocompatibility, biodegradable, renewability, low cost and non-toxicity,[14] composed mainly of highly ordered regions (crystalline structure) and disordered regions (amorphous structure), contributing to the stiffness and flexibility of the fibers, respectively.[15] This biopolymer can come from a variety of agricultural waste biomass, such as rice husk, banana, among others.[16] Thus, due to the high availability of biomass in the field, it is necessary to use alternatives for its use, aiming at the valorization of waste and the reduction of environmental impacts.[17]

In light of this, the present research investigates the interactions between three Ch[AA]IL and residual biomasses of *Oryza sativa* (rice) and *Musa cavendishii* (banana) by pretreatment, aiming to obtain nanoscale cellulose.

Experimental

Raw material and chemical composition

Rice husk (RH) and banana pseudostem (BP) biomass *in natura* were purchased from Camil Alimentos and Projeto Manoel Alves, respectively, both located in Tocantins. The RH and BP wastes were dried in an oven at 65 °C for 48 h and 60 °C for 72 h, respectively. Subsequently, they went through a milling process, using a knife mill coupled with a 20 mesh sieve and then stored in airtight bags. To obtain the cellulose and hemicellulose contents the method of Sun *et al*.[18] was used, while lignin was determined according to the methodology adapted from Sluiter *et al*.[19] The values for these biopolymers (extractive free mass) are reported in Table 1.

Table 1. Chemical composition of the biomasses

Component	Dry mass / %	
	Rice husk (RH)	Banana pseudostem (BP)
Cellulose	49.64 ± 0.92	35.86 ± 0.70
Hemicellulose	22.15 ± 0.39	24.02 ± 1.18
Lignin	24.26 ± 1.46	8.58 ± 0.64

Synthesis of ionic liquids (ILs)

For the synthesis of the ILs, 46% choline hydroxide in aqueous solution, acquired by Sigma-Aldrich, from Steinhein, Germany, and three amino acids: glycine, L-arginine and L-lysine, obtained from LabSynth, São Paulo, Brazil, were used. All reagents were used in this research, without any additional purity. The ions used in this process are shown in Table 2. The methodology followed the route used by To *et al*.,[20] with some modifications. The method consisted of reacting equimolar amounts of choline hydroxide with the amino acids under constant agitation for 3 h at a temperature of 70 ºC. After this step, the mixtures were dried under vacuum at 45 ºC.

Table 2. Reagents used in the synthesis of the ILs

Cation	Amino acid	Ionic liquid	Nomenclature
Choline hydroxide	lysine	choline lysinate	Ch[Lys]
Choline hydroxide	arginine	choline arginate	Ch[Arg]
Choline hydroxide	glycine	choline glycinate	Ch[Gly]

Fourier transform infrared spectroscopy (FTIR)

The acquisition of ILs was confirmed by Fourier transform infrared spectroscopy (FTIR) using the Agilent Technologies FTIR CARY 630, Santa Clara, United States, with the following parameters: number of scans: 8; resolution: 4 cm^{-1}; analytical range: 800-3.800 cm^{-1}. An attenuated total reflectance (ATR) cell was used.

Pre-treatment of raw materials

The pretreatment was adapted from Hou *et al*.,[11] being the main variables of the process: molar ratio, temperature and time. Thus, the samples were pre-treated by stirring in a water bath 2 mL of IL for 0.1 g of biomass. The mixture was placed in 50 mL beakers at a temperature of 100 °C for 12 h. With IL Ch[Arg], the fibers were pretreated at two temperatures: 90 and 100 °C, and these were named ARG1 and ARG respectively.

At the end of the process, the phases were separated and a co-solvent (water/ethanol) was used to remove the cellulose from the liquid phase. After cooling, the samples were centrifuged at 3000 rpm for 10 min. Subsequently, the supernatants were collected with a pipette and the liquid was stored in amber glasses for later reuse of the ionic liquid, and the filtrate was left in air for evaporation of the alcohol. The solids were washed with distilled water and ethanol using filter paper. The biomass was dried in an oven at 110 °C, and then stored in Eppendorf tubes. Figure 1 shows this step.

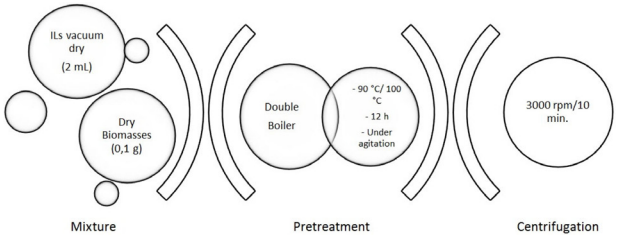

Figure 1. Conditions of the pre-treatment of the raw materials.

Sample characterization methods

Samples of rice husk and banana pseudostem (pure and pretreated) were analyzed using scanning electron microscopy (SEM). The samples were dusted over double-sided conductive carbon tape, and coated with gold using the gold film deposition system, Desk V, Denton Vacuum LLC, Moorestown, New Jersey, USA, equipped with the carbon attachment. The model JSM -6610, Jeol, Tokyo, Japan, equipped with energy-dispersive X-ray spectroscopy (EDS), Thermo scientific NSS Spectral Imaging, was used.

The transmission electron microscopy (MET) was performed in a JEM-2100 equipment, Jeol, Tokyo, Japan, equipped with EDS, Thermo Scientific, using an electron beam of 200 kV. The analyses were performed on a 2% uranyl acetate dispersion deposited on 400 mesh carbon-coated Formvar copper grids.

To obtain the XRD data, a Rigaku SmartLab SE model diffractometer, Neu-Isenburg, Germany, with a D/teX Ultra 250 detector was used. The slits used were: incident slit: ¼; length-limiting slit: 5 and 10 mm and; incident Soller slit: 2.5º. The radiation Cu Kα 1.54186 Å, operating at 40 kV and 20 mA tube voltage and current, respectively. The analysis range started at an angle of 3º and end angle of 70º, scan step 0.02º and scan speed of 5º min^{-1}.

TGA (thermogravimetric analysis), using TA Instruments, model SDT Q600, Tokyo, Japan, was operated under N_2 atmosphere at a flow rate of 100 mL min^{-1}. The heating rate we kept constant at 20 ºC min^{-1}. 5.1 mg of each sample were first heated to 105 ºC and the temperature was kept constant for 10 min to ensure complete removal of moisture. The samples were then heated to 800 ºC at a constant heating rate. Isothermal conditions were maintained at 800 ºC for another 10 min to complete the process.

Results and Discussion

Fourier transform infrared spectroscopy (FTIR)

Figure 2 shows the spectra of the three synthesized ILs: Ch[Arg], Ch[Gly] and Ch[Lys]. No representative differences were obtained between them along the wavenumber intervals. The only difference is characterized by an absorbance peak at 1635 cm^{-1} present only in Ch[Arg]. This absorption is characteristic of the quaternary ammonium group present in the colinium cation, which is usually detected at 1638 cm^{-1}, but can be reduced in the spectrum according to the ionic liquid.[21]

All ILs showed a more prominent peak in the region around 1550 cm^{-1}, in addition to broad absorption peaks

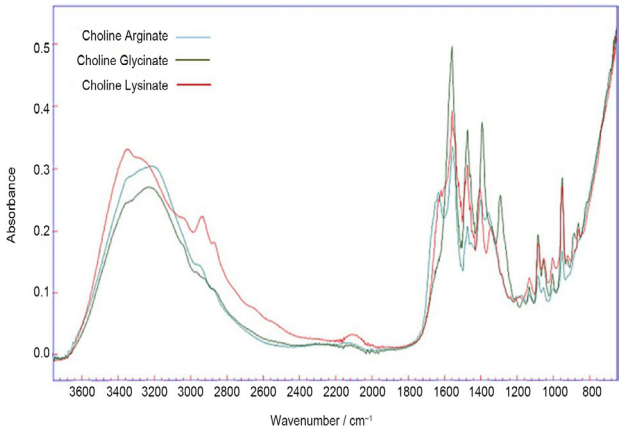

Figure 2. Infrared spectra (ATR) of the three ILs (choline arginate, choline glycinate, choline lysinate).

between 3214-3252 cm^{-1}. This sets up as something important in this research, because the absorbance band assigned to the amine group (NH_3^+), present in the investigated amino acids, is usually observed in the region 1500-1650 cm^{-1}.[22] Studying nine amino ILs, the same researchers[21] observed that the peak corresponding to the N–H stretch of NH_2 is present between 3000-3300 cm^{-1}, corroborating with the FTIR values found in the present research. Analyzing Ch[Lys] in their research, the authors[23] observed that the spectrum of the said IL exhibited a broad band between 3100 and 3450 cm^{-1} and that it is associated with OH and NH stretching.

Other absorbance peaks were identified in this research, such as 1355, 1400, and 1475 cm^{-1}, all very similar among the three ILs. Depending on the molecular constituents, carboxylate COO^- bands are generally present in the regions of 1540-1650 cm^{-1} and 1360-1450 cm^{-1}.[24] Analyzing the Ch[Lys] in FTIR, the said researchers[23] observed that the bands ranging around 1400 and 1500 cm^{-1} correspond to asymmetric and symmetric stretching vibrations of the C=O bond, and the bands between 1350 and 1470 cm^{-1}, approximately, are associated with the C–H stretching vibrations of the methyl ($–CH_3$) groups.

However, it can be inferred that the largest contribution to the FTIR spectra derives from the anions, since the spectrum of such molecules is more active due to the presence of the polar carboxylate group.[25]

Scanning electron microscopy (SEM)

Micrographs of the RH before and after pretreatment with ILs are presented in Figure 3. It is possible to infer from them that there was a disruption in the lignocellulosic structure in all pretreated samples, since the unfolded layers are noticeable when compared to the *in natura* sample. However, it was observed that the Ch[Arg] used in the

biomass in question caused greater disruption, allowing the visualization of larger and deeper pores (Figure 3b), compared to the other images (Figures 3c and 3d).

The morphology of the crude sample, therefore, shows a more compact and organized structure (Figure 3a). This is possibly due to the lignin coating on the hemicellulose and cellulose fibers.[26] After the pretreatment phase, it was observed that the biomass pretreated with Ch[Arg] caused a lighter coloration in the sample, which physically indicates that there was breakdown in the lignin, a result confirmed by SEM images. Therefore, efficient pretreatment can destroy the supramolecular structure and alter the bonding of carbohydrate and lignin matrix.[27]

The BP also showed breakage in its fibers after pretreatment as shown in Figure 4. These micrographs reveal that the pretreated fibers had their structure altered, allowing them to break. The appearance of the fibers in the waste treated with the ILs are consistent with the breaking of the bonds between the lignocellulosic biomass layers, allowing them to flake off.[28]

The original structure of this biomass presents more organized particles giving way to the pretreated biomass to more evident fibers, increasing the surface area in all samples, being evident that the ([Arg][Ch]) caused greater destructing, followed by Ch[Lys] and Ch[Gly], respectively. Investigating ILs[AA]Ch for lignin extraction

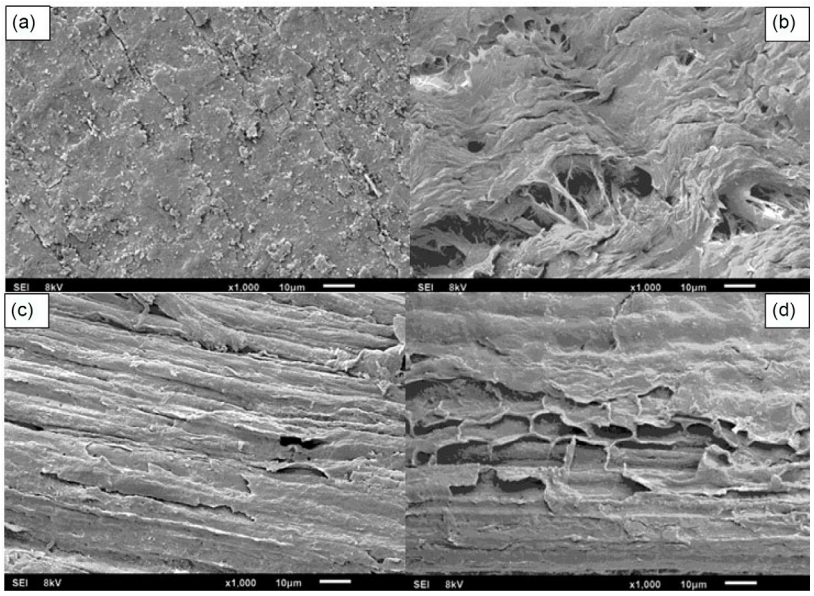

Figure 3. SEM micrographs. (a) RH *in natura*; (b) RH pretreated with Ch[Arg]; (c) RH pretreated with Ch[Gly]; (d) RH pretreated with Ch[Lys].

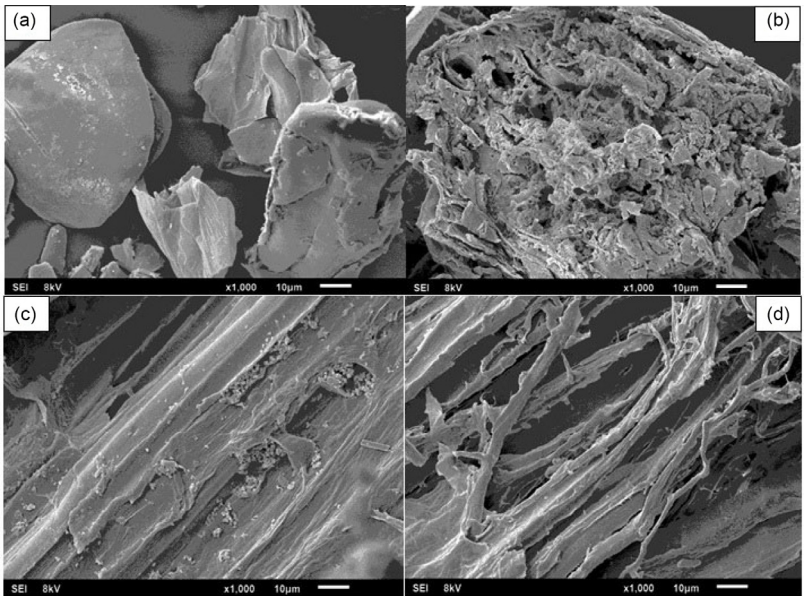

Figure 4. SEM images. (a) BP *in natura*; (b) BP pretreated with Ch[Arg]; (c) BP pretreated with Ch[Gly]; (d) BP pretreated with Ch[Lys].

from biomass, it was found that Ch[Arg] showed the best performance.[10] Computational research[29] revealed the atomic scale origin of the performance of Ch[Arg]. When conducting the studies, it was concluded that the charge group of the cation associates closely with the charge center of the anion, leading to hydrogen bond polarization, explaining the effectiveness of Ch[Arg] for biomass treatment, i.e., the strong hydrogen bonds it forms are more capable of breaking the fiber structure.

Therefore, the pretreatment step is crucial to the whole process because of its ability to improve the accessibility and reactivity of biopolymers by destroying the three-dimensional structure of lignocellulose, removing the lignin without significantly degrading the polysaccharides.[27]

Transmission electron microscopy (TEM)

TEM measurements were performed to identify the morphology and determine the diameter of the particles after pretreatment with the ILs.

The morphology of the pretreated samples (Figure 5) allowed inferring that the cellulose molecules were fragmented during pretreatment, forming interwoven fibers, with a typical conformation of nanofibrillated cellulose (NFC), however, with a smaller and less organized state of aggregation, which made difficult, for example, the exact determination of dimensions. These characteristics also reveal the removal of amorphous structures. Cellulose fiber bundles appear when lignin and hemicellulose are removed.[30]

The samples treated with Ch[Arg] presented diameters between 2 and 16 nm, showing that the pre-treatment with the mentioned IL was able to generate at least one of the dimensions on a nanometric scale, a fact that characterizes a very positive result in this research. However, the samples could not be converted into CNCs, taking into consideration that other analyses performed in this work, especially the crystallinity X-ray diffraction (XRD) did not identify crystalline samples. Furthermore, the cellulose fibers of most land plants comprise numerous individual crystalline cellulose microfibrils (approximately 3 nm wide) and their bundles.[31]

The diameter of the samples was calculated using ImageJ software[32] from approximately 100 nanofibers, and the length of the fibers could not be measured due to fiber entanglement. The curling and clustering of the fibers can influence the length of the measured fibers, in addition, the image processing tool used may be subject to error as not all fibers can be measured and as such may generate a rough approximation of the fiber length.[33]

No significant difference with respect to diameter can be detected by the TEM images between the two fibers, both show similar morphological characteristics. However, the fibers from the banana pseudostem appear in a lower state of aggregation.

Crystal characterization by X-ray diffraction

XRD was used to investigate the changes that occurred in the cellulose present in BP and RH after pretreatment.

The diffractograms corresponding to the raw and pretreated fibers are presented in Figure 6. It is possible to observe that an increase in peak intensity occurred in all

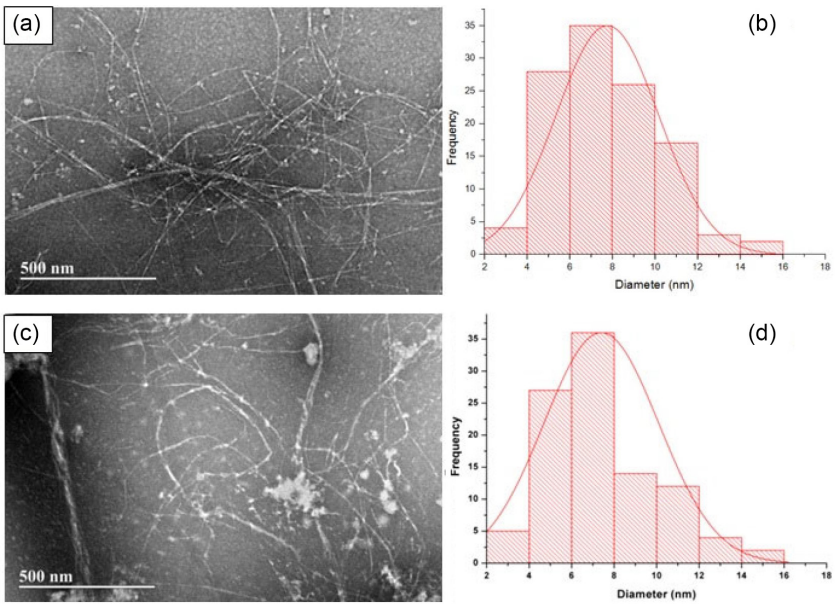

Figure 5. TEM images and histograms of nanofibers diameter distribution. (a) Morphology of RH fibers treated with Ch[Arg]; (b) diameter of RH fibers; (c) morphology of BP fibers treated with Ch[Arg]; (d) diameter of BP fibers.

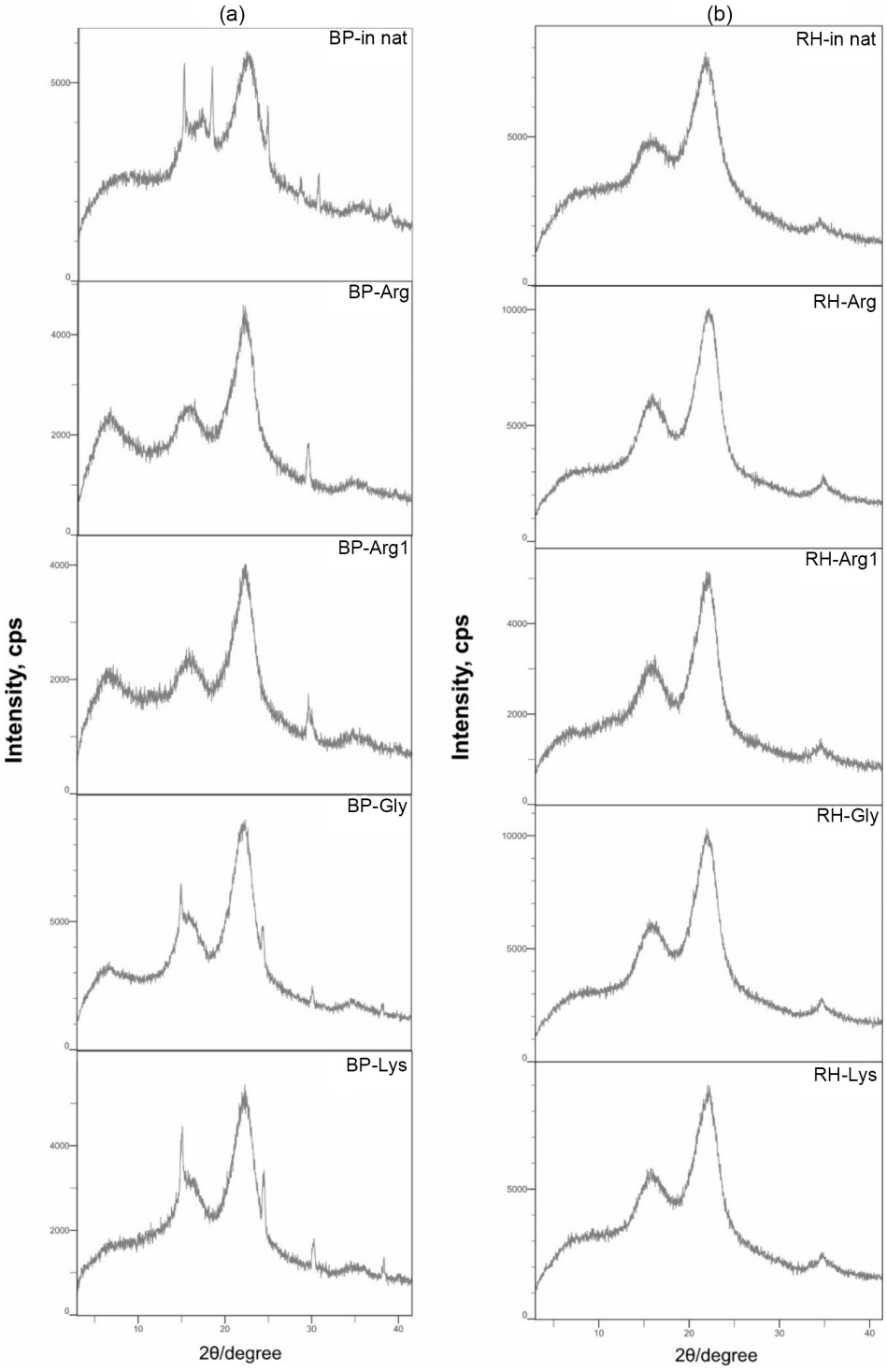

Figure 6. Diffractograms of the biomasses. (a) BP; (b) RH.

samples pretreated with the ILs, inferring that lignin and hemicellulose were affected, as identified in SEM analyses previously. The diffractograms with narrower and sharper peaks is due to their higher crystallinity compared to other samples.[34]

The removal of amorphous components, however, may have been in lower amounts, being unable to generate crystallinity, since the samples present amorphous pattern. Corroborating this result, the literature[30] presents XRD analyses of amorphous samples, similar to the diffractograms reported in this scientific research. Nanocellulose is obtained when the action of the chemical used breaks down the amorphous regions of cellulose, which are structurally more disordered than the crystalline

regions.[30] The ordered and crystalline nature of cellulosic fibers that makes them highly recalcitrant also represents one of the main impediments to the deconstruction of lignocellulose.[35]

In the diffraction patterns in this research, it is possible to notice that the RH samples presented some differences in the behavior of the peaks with respect to the raw sample. The fraction around 2θ = 16º appears more intense and evident in the pretreated samples, especially in the fiber treated with Ch[Arg]. In addition, all the peaks at 2θ = 22º appear with higher intensity. Thus, diffractograms that exhibit a well-defined main peak around 2θ = 22.6° is characteristic of cellulose I.[36]

The highest intensities in the diffractograms referring to BP occur at 2θ = 22.5º. When compared to the crude sample, all pretreated samples show the formation of a new peak at 2θ = 7º, in addition to a more intense peak around 2θ = 29º only in the samples pretreated with Ch[Arg]. Many peaks present in the crude sample (2θ = 15, 17, 18, 24º) disappear in the samples pretreated with this IL.

In addition, it can be seen that the 100 °C temperature tested at Ch[Arg] showed a higher peak intensity when compared to the 90 °C temperature for both species. Thus, it is possible to infer that cellulose crystallinity can occur at a higher temperature. Another factor that may have had an influence on the pretreated cellulose is the molar ratio of the substances used. Different molar ratios of solvents can affect the crystallinity of pretreated biomass samples.[27]

To isolate cellulose nanocrystals, it is important to remove the lignin and hemicellulose fractions as much as possible, since the stiffness of the highly crystalline cellulose particles cannot be fully exploited if they remain embedded in the amorphous cementing materials, i.e., lignin and hemicellulose.[5]

Thermogravimetric analysis (TGA)

TGA was performed to identify the rate of degradation of lignocellulosic biomasses, in addition to the structural composition. This methodology measures mass loss over time as a function of temperature.[37]

In the thermogravimetry curves, it is possible to observe two well-defined stages of mass loss in the cellular composition of the two fibers studied. All thermograms show a small mass loss that varies between 23 and 100 °C. The initial mass loss of the fibers occurs below 140 °C and is attributed to the reduction of moisture content in the lignocellulosic fibers.[38] Moreover, this first temperature range between 25 and 100 °C is related, besides the evaporation of water, to the elimination of some volatile compounds.[39]

The second mass loss is more intense, with some differences between the species. In the thermogram referring to BP (Figure 7), the crude fiber presents besides the two stages observed in the fresh sample, two more rapid and less prominent decays (one around 149 ºC and another at approximately 429 ºC). Furthermore, the pretreated samples begin their degradation process at higher temperatures than the fresh sample, presenting, therefore, a greater thermal stability.

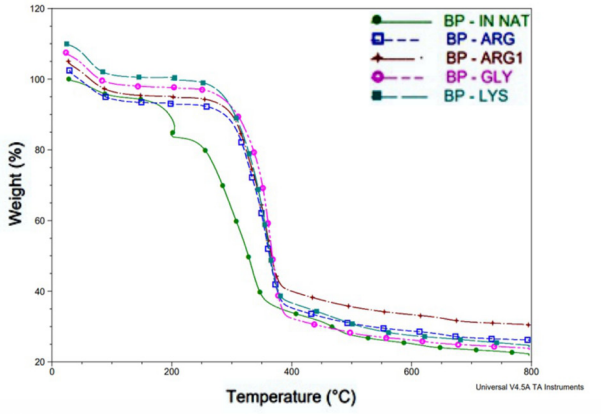

Figure 7. Thermal decomposition of crude and pretreated BP.

The sample that presents a higher thermal stability is BP-Arg, which starts its most accentuated degradation stage at 255.19 ºC and ends at 387.80 ºC, with mass loss of 56%, while the fiber BP-*in natura* starts its degradation at 232.91 ºC and ends at 359.15 ºC, with mass loss equal to 45%. These degradation values refer to hemicellulose and cellulose, respectively. Hemicellulose is known to decompose easily, recording mass loss at temperatures ranging from 220 to 325 °C.[40] The temperatures and mass losses for all pretreated samples are presented in Tables 3 and 4.

Table 3. Temperatures and mass losses of the sharpest curve in the banana pseudostem (BP)

Biomass-IL	IT / °C	FT / °C	Mass loss / %
BP-*in natura*	232.91	359.16	45
BP-Arg	255.19	387.80	56
BP-Arg1	252	387	53
BP-Lys	250.94	384.62	61
BP-Gly	250.94	394.17	64

IL: ionic liquid; IT: initial temperature; FT: final temperature.

The thermogram for RH (Figure 8) shows that the second phase began with the decay at an initial temperature corresponding to 223.36 ºC and continued until 393.10 ºC for RH IN NAT, resulting in a mass loss of 55%. The fiber that showed a higher thermal stability was RH ARG whose

Table 4. Temperatures and mass losses of the sharpest curve in rice husk (RH)

Biomass-IL	IT / °C	FT / °C	Mass loss / %
RH-*in natura*	223.36	393.10	55
RH-Arg	252	388	64
RH-Arg1	248.82	388.86	64
RH-Lys	246.7	394.2	55
RH-Gly	236.09	393.10	60

IL: ionic liquid; IT: initial temperature; FT: final temperature.

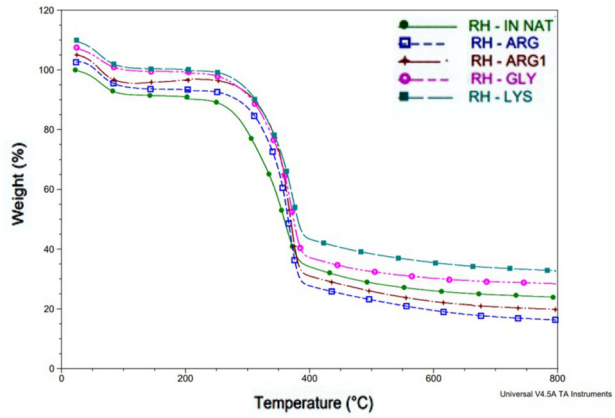

Figure 8. Thermal decomposition of fresh and pretreated RH.

degradation process starts at 252 ºC and ends at 388 ºC totaling mass loss in the value of 64%. The *in natura* sample also presents a rapid and small inclination around 202.14 ºC.

In this second step, therefore, the decomposition of hemicellulose and cellulose occurred, since both can occur concomitantly. Hemicellulose and cellulose follow a similar decomposition pattern, with slightly lower activation and decomposition temperatures in the case of hemicellulose.[30] For the same authors,[30] the decomposition of hemicellulose, cellulose and lignin, occurs between 220 and 550 °C.

Thus, among the three main constituents of the fiber, lignin stands out as the most difficult to decompose, which degrades slowly up to the range of 900 ºC.[41] In this research, it was not possible to identify the process of lignin degradation, with the exception of the BP-*in natura* sample that shows a fourth and slight decay around 429 to 494 ºC with a mass loss equal to 4%. These results are in agreement with the thermal decomposition of natural fibers, which begins with the decomposition of hemicellulose (200 to 260 °C), cellulose (240 to 350 °C), and lignin (280 to 500 °C).[42]

Conclusions

The results confirmed the spectra corresponding to the ions proving the synthesis of the ILs effectively.

The SEM measurements revealed structural transformations in the two tested lignocellulosic fibers, showing that the pretreatment with the Ch[AA]ILs influenced the destructing of the biomasses. In addition, the morphology of the samples seen in TEM allowed inferring that the ILs were efficient, being able to generate CNFs with nanometer-scale diameter size.

The diffractograms obtained revealed increased peaks in all pretreated samples when compared to the raw fibers, although no crystalline samples could be formed.

All pretreated samples showed differences with respect to crude fiber according to TGA, with the biomasses treated with IL Ch[Arg] showing higher thermal stability in both species.

The banana pseudostem and rice husk presented important characteristics during pretreatment, configuring themselves as potential sources of waste for use in various applications as a biomaterial. However, the BP, due to its lower lignin content, made the surface morphology more favorable, demonstrating a correlation between the chemical composition of the fibers and its positive influence on them.

Of the three ILs tested, Ch[Arg] was able to most effectively solubilize the pretreated biomasses, followed by Ch[Lys] and Ch[Gly], respectively.

Author Contributions

Fabiane F. Silva was responsible for data curation, investigation, methodology, writing original draft; Danylo B. Mendes for data curation, formal analysis, software; Patrícia M. Guarda for visualization, writing review and editing; Anselmo F. Ruiz Rodriguez for formal analysis, software; Emerson Adriano Guarda for data curation, formal analysis, methodology, supervision, validation, writing review and editing.

References

1. Welton, T.; *Biophys. Rev*. **2018**, *10*, 691. [Crossref]
2. Equihua-Sanchez, M.; Barahona-Perez, L. F.; *Waste Biomass Valorization* **2019**, *10*, 1285. [Crossref]
3. Haron, G. A. S.; Mahmood, H.; Noh, H. B.; Goto, M.; Moniruzzaman, M.; *J. Mol. Liq.* **2022**, *346*, 118208. [Crossref]
4. Zinge, C.; Kandasubramanian, B.; *Eur. Polym. J.* **2020**, *133*, 109758. [Crossref]
5. Adil, S. F.; Bhat, V. S.; Batoo, K. M.; Imran, A.; Assal, M. E.; Madhusudhan, B.; Khan, M.; Al-Warthan, A.; *J. Saudi Chem. Soc.* **2020**, *24*, 374. [Crossref]
6. Thomas, B.; Raj, M. C.; Joy, J.; Moores, A.; Drisko, G. L.; Sanchez, C.; *Chem. Rev.* **2018**, *118*, 11575. [Crossref]
7. Woiciechowski, A. L.; Dalmas Neto, C. J.; Porto de Souza, V. L.; de Carvalho Neto, D. P.; Novak, A. C. S.; Letti, L. A. J.; Karp,

S. G.; Zevallos, L. A. T.; Soccol, C. R.; *Bioresour. Technol.* **2020**, *304*, 122848. [Crossref]
8. Draszewski, C. P.; Bragato, C. A.; Lachos-Perez, D.; Celante, D.; Frizzo, C. P.; Castilhos, F.; Tres, M. V.; Zabot, G. L.; Abaide, E. R.; Mayer, F. D.; *J. Supercrit. Fluids* **2021**, *178*, 105355. [Crossref]
9. Gontrani, L.; *Biophys. Rev.* **2018**, *10*, 873. [Crossref]
10. An, Y.; Zong, M.; Wu, H.; Li, N.; *Bioresour. Technol*. **2015**, *192*, 165. [Crossref]
11. Hou, X.-D.; Xu, J.; Li, N.; Zong, M.; *Biotechnol. Bioeng.* **2015**, *112*, 65. [Crossref]
12. Papa, G.; Feldman, T.; Sale, K. L.; Adani, F.; Singh, S.; Simmons, B. A.; *Bioresour. Technol.* **2017**, *241*, 627. [Crossref]
13. Ziaei-Rad, Z.; Pazouki, M.; Fooladi, J.; Azin, M.; Gummadi, S. N.; Allahverdi, A.; *Sci. Rep.* **2023**, *13*, 446. [Crossref]
14. Du, H.; Liu, W.; Zhang, M.; Si, C.; Zhang, X.; Li, B.; *Carbohydr. Polym.* **2019**, *209*, 130. [Crossref]
15. Dahlem Jr., M. A.; Borsoi, C.; Hansen, B.; Catto, A. L.; *Carbohydr. Polym.* **2019**, *218*, 78. [Crossref]
16. Merais, M. S.; Khairuddin, N.; Salehudin, M. H.; Mobin Siddique, M. B.; Lepun, P.; Chuong, W. S.; *Membranes* **2022**, *12*, 451. [Crossref]
17. Uchôa, P. Z.; Porto, R. C. T.; Battisti, R.; Marangoni, C.; Sellin, N.; Souza, O.; *Ind. Crops Prod.* **2021**, *174*, 114. [Crossref]
18. Sun, X. F.; Sun, R. C.; Fowler, P.; Baird, M. F.; *Carbohydr. Polym.* **2004**, *55*, 379. [Crossref]
19. Sluiter, A.; Hames, B.; Ruiz, R.; Sacarlata, C.; Sluiter, J.; Templeton, D.; Crocker, D.; *Determination of Structural Carbohydrates and Lignin in Biomass*; National Renewable Energy Laborator of Analytical (NREL): Golden, USA, 2008. [Link] accessed in April 2024
20. To, T. Q.; Shah, K.; Tremain, P.; Simmons, B. A.; Moghtaderi, B.; Atkin, R.; *Fuel* **2017**, *202*, 296. [Crossref]
21. Korban, A. M.; Moshikur, R. M.; Wakabayashi, R.; Tahara, Y.; Moniruzzaman, M.; Kamiya, N.; Goto, M.; *J. Colloid Interface Sci.* **2019**, *551*, 72. [Crossref]
22. Sistla, Y. S.; Khanna, A.; *Chem. Eng. J.* **2015**, *273*, 268. [Crossref]
23. Villar-Chavero, M. M.; Domínguez, J. C.; Alonso, V. M.; Rigual, V.; Mercedes, O.; Rodriguez, F.; *Int. J. Biol. Macromol.* **2019**, *133*, 262. [Crossref]
24. Martins, C. F.; Neves, L. A.; Chagas, R.; Ferreira, L. M.; Afonso, C. A. M.; Coelhoso, I. M.; Crespo, J. G.; Mota, J. P. B.; *Chem. Eng. J.* **2021**, *421*, 127875. [Crossref]
25. Scarpellini, E.; Ortolani, M.; Nucara, A.; Baldassarre, L.; Missori, M.; Fastampa, R.; Caminiti, R.; *J. Phys. Chem.* C **2016**, *120*, 24088. [Crossref]
26. Financie, R.; Moniruzzamana, M.; Uemura, Y.; *BioChem. Eng. J.* **2016**, *110*, 1. [Crossref]
27. Xu, H.; Peng, J.; Kong, Y.; Liu, Y.; Su, Z.; Li, B.; Song, X.; Liu, S.; Tian, W.; *Bioresour. Technol*. **2020**, *310*, 123416. [Crossref]
28. Brunner, M.; Li, H.; Zhang, Z.; Zhang, D.; Atkina, R.; *Fuel* **2019**, *236*, 306. [Crossref]
29. Karton, A.; Brunner, M.; HowarD, M. J.; Warr, G. G.; Atkin, R.; *ACS Sustainable Chem. Eng.* **2018**, *6*, 4115. [Crossref]
30. Orrabalis, C.; Rodríguez, D.; Pampillo, L. G.; Londoño-Calderón, C.; Trinidad, M; Martínez-García, R.; *Mater. Res.* **2019**, 22, e20190243. [Crossref]
31. Ono, Y.; Takeuchi, M.; Isogai, A.; *Cellulose* **2022**, *29*, 9105. [Crossref]
32. Rasband, W. S.; *ImageJ*; U. S. National Institutes of Health, Bethesda, Maryland, USA, 2015. [Link] accessed in May 2024
33. Madivoli, E. S.; Kareru, P. G.; Gachanja, A. N.; Mugo, S. M.; Makhanu, D. S.; *SN Appl. Sci.* **2019**, *1*, 273. [Crossref]
34. Teixeira, M. E.; Corrêa, A. C.; Manzoli, A.; Leite, F. L.; Oliveira, C. R.; Mattoso, L. H. C.; *Cellulose* **2010**, *17*, 595. [Crossref]
35. Roy, S.; Chundawat, S. P. S.; *BioEnergy Res.* **2023**, *16*, 263. [Crossref]
36. Klemm, D.; Heublein, B.; Fink, H. P.; Bohn, A.; *Angew Chem., Int. Ed.* **2005**, *44*, 3358. [Crossref]
37. Ibrahim, M. I. J.; Sapuan, S. M.; Zainudin, E. S.; Zuhri, M. Y. M.; *Bio. Res.* **2019**, *14*, 6485. [Crossref]
38. Meng, F.; Wang, G.; Du, X.; Wang, Z.; Xu, S.; Zhang, Y.; *Composites* **2019**, *160*, 341. [Crossref]
39. Hafemann, E.; Battisti, R.; Bresolin, D.; Marangoni, C.; Machado, R. A. F.; *Waste Biomass Valorization* **2020**, *11*, 6595. [Crossref]
40. Yang, H.; Yan, R.; Chen, H.; Lee, D. H.; Zheng, C.; *Fuel* **2007**, *86*, 1781. [Crossref]
41. Silva, F. S.; Ribeiro, C. E. G.; Demartini, T. J. C.; Rodríguez, R. J. S.; *Macromol. Symp*. **2020**, *394*, 2000052. [Crossref]
42. Lomelí-Ramírez, M. G.; Kestur, S. G.; Manríquez-González, R.; Iwakiri, S. M. G. B.; Flores-Sahagun, T. S.; *Carbohydr. Polym.* **2014**, *102*, 576. [Crossref]

Submitted: January 13, 2024
Published online: May 14, 2024